Electrocatalysis (2019) 10:332–341
https://doi.org/10.1007/s12678-019-0511-9

ORIGINAL RESEARCH

Pd, PdSn, PdBi, and PdBiSn Nanostructured Thin Films for the Electro-Oxidation of Ethanol in Alkaline Media

Nqobile Xaba[1,2] · Remegia M. Modibedi[1] · Mkhulu K. Mathe[1] · Lindiwe E. Khotseng[2]

Published online: 11 February 2019

Abstract

Pd, PdSn, PdBi and PdBiSn nanostructured thin films were prepared on Au substrate using the electrochemical atomic layer deposition technique. The activity of the nanostructured thin films towards the electro-oxidation of ethanol was tested in alkaline media using electrochemical methods. Scanning electron microscopy results showed that the nanoparticles were evenly distributed on the surface, while the elemental analysis confirmed the presence of all elements on the prepared materials. Cyclic voltammetry studies revealed that the addition of Sn and Bi on Pd improved the activity of Pd and that the ternary nanostructured catalyst was more active towards the oxidation of ethanol than the binary catalysts.

Keywords Electrodeposition · Thin films · Electro-oxidation · Ethanol

Introduction

Alkaline fuel cells (AFCs) and proton exchange membrane fuel cells (PEMFCs) have been extensively studied amongst other fuel cell types due to their potential applications in portable electronic and automobile industry. AFCs also have several advantages over PEMFCs on both faster cathode kinetics and Ohmic polarisation. Moreover, the alkaline environment, which is less corrosive, ensures a longer durability and the use of non-noble cheap oxygen reduction reaction electrocatalysts cuts down the costs of the fuel cell drastically. Therefore, AFCs can theoretically outperform PEMFCs. A major limitation of AFCs however is the progressive carbonation of the alkaline electrolyte due to CO_2 formation from air or the oxidation product of the fuel. This problem was addressed mainly by the application of anion exchange membranes (AEMs) [1–6]. Over the past decade, alkaline direct alcohol fuel cells (ADAFCs) have attracted increasing interest due to the favourable reaction kinetics in alkaline media, easy handling of the liquid fuels and the higher energy densities achievable. ADAFCs using AEMs have several advantages over conventional alkaline fuel cells, such as (1) no electrolyte leaking, (2) since there is no mobile cation, there is no precipitated carbonate, (3) reduced alcohol crossover, (4) potential simplified water management due to the fact that water is produced at the anode and consumed at the cathode and (5) potentially reduced corrosion [1, 7].

The oxidation of alcohols is necessary for energy production and this requires breaking the C-C bonds which is difficult to do [8, 9]. The main catalyst used in the electro-oxidation of alcohols is Pt catalysts, and this has been done in acidic media. The extensive use of Pt catalysts is not economically viable due to Pt cost, the slow kinetics of the reaction, and also the CO poisoning of the catalyst [10, 11]. Pd-based catalysts in basic media are great alternatives. Pd and Pt have similar chemistries (same group elements). The electro-oxidation reaction of ethanol using Pd in alkaline media is limited by slow kinetics. The rate is limited by the removal of adsorbed acetyl species by reacting with hydroxyl species forming acetates [8, 10]. A minor quantity of the acetyl species goes towards decomposition to form hydrocarbons and carbon monoxide further oxidised to carbon dioxide.

Pd-based catalysts have been investigated for the alcohol oxidation reaction (AOR) in alkaline media, and further research still needs to be done to improve activity, selectivity and stability of the catalysts [6, 11–16]. This can be done by

✉ Remegia M. Modibedi
mmodibedi@csir.co.za

[1] Energy Materials, Energy Centre, Council for Scientific and Industrial Research (CSIR), Pretoria, South Africa

[2] Department of Chemistry, University of Western Cape, Private Bag X17, Bellville 7535, South Africa

formation of nanosized catalysts for high surface area, and the addition of other elements to Pd to improve catalytic activity. Electrochemical atomic layer deposition (E-ALD) allows the formation of well ordered, tailor made, and thin films material using monolayer formation on well-ordered surfaces using underpotential deposition and surface-limited redox reactions [17]. The formation of Pd nanostructures on Au substrates is well covered in literature [18–23].

Ethanol is attracting great attention as fuel since it is less toxic than methanol and can be massively produced from agricultural products or biomass, in addition to the advantage of high-specific energy [24]. Hence, tremendous efforts have been made to the development of alkaline direct ethanol fuel cells (ADEFCs). Ethanol has also been proven by research to have a lower crossover rate and affects the cathode performance less severely than methanol [25]. This study aims to fabricate PdSn, PdBi and PdBiSn thin films on Au substrate using E-ALD technique. Pd was prepared via surface limited replacement reaction (SLRR) of underpotential (UPD) deposited Cu on Au electrode. Pd containing Sn and or Bi was deposited using SLRR of Cu UPD followed by direct UPD of Sn or Bi. The deposition cycle used was developed from the study of the reduction and oxidation of each element using cyclic voltammetry. The formed material was characterised using field emission scanning electron microscope (FESEM) for morphology equipped with energy dispersive detector (EDS) for the elemental analysis. The activity of each material towards the oxidation of ethanol and glycerol was investigated using cyclic voltammetry.

Experimental Procedure

Materials and Reagents

High purity (≤ 1 μS/cm) deionised water and ACS Reagent grade chemicals (Sigma-Aldrich) were used in the preparation of all solutions. The chemical solutions prepared were as follows: 0.1 mM $PdCl_2$ in 0.5 M HCl, 1 mM $CuSO_4$ in 0.1 M H_2SO_4, 0.2 mM SnO in 0.1 M H_2SO_4 and 0.2 mM Bi_2O_3 in 0.1 M H_2SO_4.

Substrate Treatment

Au-coated glass slides containing 100 nm Au film on 5 nm Ti on glass (evaporated metal films, Ithaca, NY) were used as substrate. Prior use, they were cleaned by sonication in acetone for 5 min, deionised water rinse, dipped in concentrated HNO_3 for 2 min, deionised water rinse and finally dried with nitrogen.

E-ALD Deposition

The substrate was placed into the electrochemical flow cell and immediately further cleaned by flushing with 0.1 M H_2SO_4 while the potential of the cell was alternated three times between 1400 mV and − 200 mV. A three-electrode electrochemical flow cell was used during the deposition. Au wire and Ag/AgCl (3 M KCl) (MF-2021, BASI) served as auxiliary and reference electrodes, respectively. Copper tape was used as mode of contact for the working electrode (Au-coated glass). The solutions were degassed with nitrogen gas for at least 60 min and then pumped through master flex tubes from their reservoirs using a peristaltic pump. A rubber gasket was used to limit the surface of the Au electrode to 2.1 cm^2. The deposition conditions were studied and optimised using cyclic voltammetry and analysis of current-potential time plots.

Electrodeposition of Pd-Based Materials on Au Substrate

The electrodeposition of Pd-based materials was done using Cu UPD on Au substrate was adapted from the work done by Mkwizu and co-workers [26], and Modibedi et al. [12], as well as other sources [27, 28]. It was carried out as follows: (i) pump the Cu solution into the cell at an applied potential (E_{app}), (ii) keep the Cu solution in the flow cell to deposit Cu at E_{app}, (iii) pump Pd solution into the cell at open circuit potential (E_{ocp}), (iv) keep Pd solution in the cell for deposit Pd (SLRR) at E_{ocp} and (v) rinse with electrolyte at E_{ocp}. This cycle was repeated as many times as required to form the deposit. Pd materials containing Sn and Bi were formed by introducing a second element in the following steps and depositing it at UPD as described below.

Electrodeposition of Sn and Bi on Au Substrate

The deposition cycle that was used to form a layer of Bi or Sn is described. A deposit of Bi involved these steps: (i) flow Bi^{3+} solution at − 50 mV for 10 s, (ii) deposit Bi at − 150 mV for 5 s and (iii) rinse in 0.1 M H_2SO_4 at − 150 mV. A similar cycle was used to deposit Sn as follows: (i) flow Sn^{2+} solution at − 50 mV for 15 s, (ii) deposit Sn at − 425 mV for 5 s and (iii) rinse in 0.1 M H_2SO_4 at − 425 mV for 15 s. Sn or Bi was deposited first or followed a layer of electrodeposited Pd, and the formed deposits are listed in Table 1.

Characterisation

The electrochemical activity of the prepared Pd-based catalysts was evaluated using an electrochemical flow cell with three electrode system as described in literature [12, 27, 29]. Cyclic and linear sweep voltammetry in N_2 saturated 0.1 M KOH, and 0.1 M EtOH on a potentiostat Metrohm

Table 1 List of Pd-based materials catalyst deposition description charge for the prepared catalysts in 0.1 M KOH

Material	Sequence	Number of cycles	Charge/C
Pd	Cu UPD; Pd SLRR at OCP; ×25 cycles	25	1.50E-05
PdSn	Cu UPD; Pd SLRR, Sn UPD; ×25 cycles	25	7.57E-06
PdBi	Cu UPD; Pd SLRR; Bi UPD; ×25 cycles	25	1.32E-05
PdBiSn 30	(i) Cu UPD; Pd SLRR; Bi UPD; ×15 cycles; (ii) Cu UPD; Pd SLRR; Sn UPD; ×15 cycles	30	6.88E-06
SnPd	Sn UPD; Cu UPD; Pd SLRR; ×25 cycles	25	5.12E-06
BiPd	Bi UPD; Cu UPD; Pd SLRR; ×25 cycles	25	1.07E-05
PdBiSn 25	(i) Cu UPD; Pd SLRR; Bi UPD; ×13 cycles; (ii) Cu UPD; Pd SLRR; Sn UPD; ×12 cycles	25	5.10E-06

PGSTAT101 controlled by NOVA 1.8 software was conducted. The morphology of the materials was evaluated using a scanning electron microscope performed on a LEO 1525 field emission scanning microscope (FE-SEM) with the acceleration voltage of 2.00 kV, and equipped with dispersive detector (EDS) for elemental mapping.

Results and Discussion

Electrodeposition of Various Pd on Au Catalysts

The characteristic cyclic voltammogram (CV) of 1 mM $CuSO_4$ in 0.1 M H_2SO_4 on Au electrode is shown in Fig. 1a. The scan began at 0.35 V negatively until a lower limit of − 0.35 V and reversed. The negative scan shows a bulk deposition peak onset at − 0.025 V and the corresponding bulk stripping peak at 0.05 V. The insert graph A shows the UPD region where it was found to occur between 0.2 and 0 V. This is consistent to the values reported in literature [27, 28, 30]. The obtained Cu UPD (Fig. 1b) was used to form a Pd deposition cycle, where Pd was deposited at a set potential, followed by replacement with Pd at open circuit potential. The deposition cycle was made up of the following steps: (i) pump Cu^{2+} solution for 15 s at OCP; (ii) deposit Cu at 50 mV for 10 s at 150 mV; (iii) pump Pd^{2+} solution for 15 s at OCP; (v) hold the solution at OCP for 10 s and (iv) rinse in blank for 15 s at OCP.

The cycle was repeated 25 and 50 times for film growth. The formation of Pd-based catalysts containing Sn and Bi will be done by building from the above deposition cycle. The cyclic voltammograms of Bi^{3+} and Sn^{2+} are shown in Fig. 1c, d respectively with an insert of Au electrode CV, where the UPD of Bi^{3+} and Sn^{2+} was found to be at 50 mV and − 325 mV respectively. A characteristic cyclic voltammogram of the Au electrode in 0.1 M H_2SO_4 negative scan shows reduction peak corresponding to the reduction of Au_2O_3 to Au (peak A) [31] and turned at − 200 mV before hydrogen evolution peak could appear. The reverse scan continued until a potential of 1400 mV was reached. This results in the appearance of the oxidation peaks, indicating the oxidation of surface Au atoms from different crystallographic planes (peaks B). The window opening cyclic voltammetry study of Bi deposition on Au in 0.2 mM Bi^{3+} solution is shown in Fig. 1c. All CV curves were scanned negatively and then reversed. There are three oxidation peaks observed at approximately 0 mV, 150 mV and 275 mV (peaks c, d and e). The area of peak at 0 mV increased when scanned more negatively, indicating bulk Bi deposition. The latter two peaks had the same peak height regardless of increasing the negative potential. These peaks are representative of the UPD oxidation peaks. UPD processes are not dependent on potential change because they are surface limited reactions. The study of Sn deposition on Au in 0.2 mM Sn2+ solution is shown in the window opening CV shown in Fig. 1d. The potential was scanned from open circuit potential and held at different negative limits for 30 s to force the stripping peak of Sn to appear. As a result, no reductive regions were observed on the scan, only two oxidative features were visible at − 200 mV and 0 mV (peaks A and B). The onset UPD potential was found to be at − 350 mV which slowly grew to bulk deposition at − 425 mV and beyond.

The information obtained from the CV studies was used to deduce a deposition cycle for catalysts materials containing Pd, Sn and Bi. Materials made up of PdSn, PdBi and PdBiSn were made using the above deposition cycle followed by Sn or Bi UPD or both. The binary catalyst PdSn deposition cycle steps were as follows: (i) pump Cu^{2+} solution for 15 s at OCP; (ii) deposit Cu for 10 s at 50 mV; (iii) pump Pd^{2+} solution for 15 s at OCP; (v) hold the solution at OCP for 10 s; (iv) rinse in blank for 15 s at OCP; (vi) pump Sn^{2+} solution for 15 s at OCP; (vii) deposit Sn at for 10 s at − 325 mV and (viii) rinse in blank for 15 s at OCP. A similar deposition cycle was used for PdBi by replacing Sn UPD with Bi UPD of 50 mV. The formation of a material by alternating Pd SLRR followed by Bi and Sn at UPD was unable to form a deposit, due to Sn and Bi UPD being too far apart. The summary of the deposition sequence for each material is given in Table 1.

This resulted in the ternary material deposition cycles being designed to avoid this by depositing Pd and Bi first, followed

by depositing Pd and Sn, using the PdBi cycle and then the PdSn cycle. Two materials were made namely PdBiSn 25 and PdBiSn 30. The ternary PdBiSn 30 was deposited using a sequence made up of the PdBi cycle repeated 15 times followed by the PdSn cycle repeated 15 times. The PdBiSn 25 was made by depositing PdBi 13 time and PdSn 12 times. The possibility of depositing Sn or Bi on top of the Pd layer to form PdSn or PdBi was explored. A CV of Cu^{2+} UPD on Bi and Sn deposited on Au monolayer (Fig. 1b) showed that the Cu^{2+} UPD has not changed. This resulted in the deposition cycle for SnPd and BiPd being the reverse of PdSn and PdBi. A visible deposit for BiPd was not able to form.

Structural Characterisation

The morphology of the formed deposits was investigated using SEM. The Pd deposits were found to have rounded particles clustered all over the surface; in some areas, they were found to agglomerate as illustrated in Fig. 2a, b, and the deposit was found to contain Pd distributed all over the surface as shown on the map (Fig. 2c–e) and spectra (Fig. 2f). Pd deposits form larger structures on the surface and this is prominent when the number of cycles was increased or for thicker deposits as shown in Fig. 3a, b. PdSn and SnPd deposits (Fig. 3c, d) were found to have similar characteristics to each other, where smaller particles are dominant on the surface and few larger randomly distributed particles. Elemental map did not reveal any differences in particle composition. The PdBi deposits (Fig. 3d) were found to contain well-rounded larger particles on the surface distributed evenly as well were smaller particles.

The elemental map indicated that the surface was evenly covered with Pd and Bi. PdBiSn 25 was also similar structurally to the other catalysts (Fig. 3f), and the elemental map of PdBiSn 25 in Fig. 4a–d and spectra (Fig. 4e) shows the presence of Pd, Sn and Bi on the surface directly on top of each other all over the surface. When comparing all the materials, only the PdBi materials exhibited a different morphology to the rest of the prepared materials.

Electrochemical Characterisation

The cyclic voltammograms of the Pd and Pd-modified catalysts in 0.1 M KOH solution are presented in Fig. 5a, b. The peaks

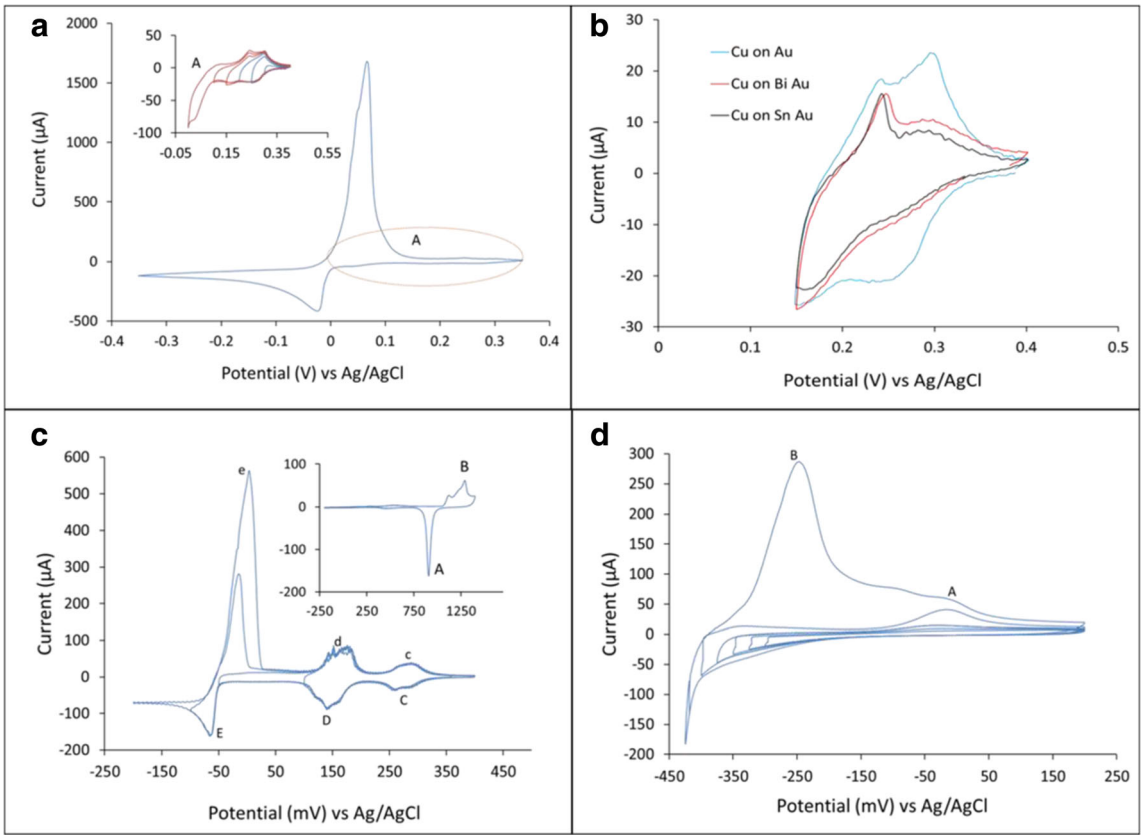

Fig. 1 **a** Cyclic voltammogram of 1 mM $CuSO_4$ in 0.1 M H_2SO_4 on Au at a scan rate of 10 mV/s, and an insert of the window opening. **b** Cyclic voltammogram of 1 mM $CuSO_4$ in 0.1 M H_2SO_4 on Bi covered Au, and Sn covered Au, at a scan rate of 10 mV/s. **c** Cyclic voltammograms of Au electrode in 0.2 mM Bi_2O_3 vs Ag/AgCl, and an insert of Au electrode in 0.1 M H_2SO_4, at a scan rate of 10 mV/s. **d** Cyclic voltammograms of Au electrode in 0.2 mM SnO vs Ag/AgCl, at a scan rate of 10 mV/s

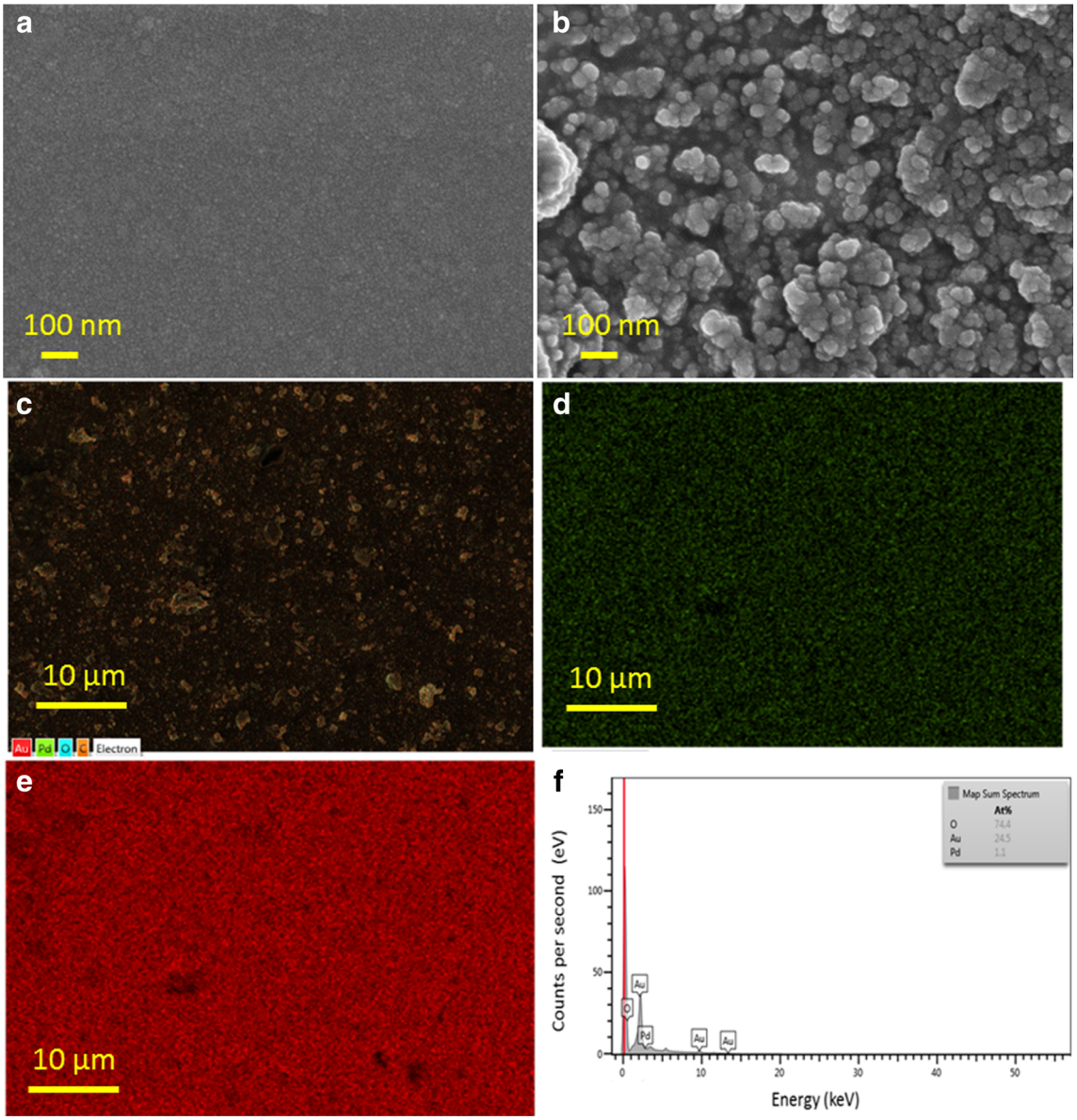

Fig. 2 SEM images of **a**, **b** Pd/Au 25 at different magnification, **c** Pd catalysts overlaid elemental map, **d** Pd elemental map, **e** Au elemental map and **f** EDS spectrum

found below − 0.8 V onwards are due hydrogen absorption and adsorption on Pd surface. Au is not prone to hydrogen evolution reactions [11] hence no peaks were observed for Au. The oxidation peaks found at 0 V and above is due to the oxidation of Au oxides. The reduction peak observed in the region of 0 V towards − 0.3 V is caused by the reduction of the Pd oxides. This peak is different for all the catalysts, indicating that the modified catalysts have different electrochemical activity. The Pd on Au catalyst exhibited the most pronounced peaks in the hydrogen evolution region (− 0.8 V and below), and a higher charging current. The CV shows the signature of Pd in alkaline electrolyte [32]. The SnPd and PdBiSn 25 catalyst had the exact same interaction with KOH, as indicated by their cyclic voltammograms matching. The reduction peaks for all the catalysts occurred at different potentials implying that all the material has a different Pd dispersion on the surface. The current associated with this reduction peak is directly proportional to the charge required to reduce Pd oxides as shown in Eq. 1 used to calculate the electrochemical active surface (EAS) of the catalyst [11, 32]. The charge obtained by integrating the area under the Pd reduction peak is shown in Table 1. The results shows that BiPd has the highest charge, followed by PdBi, the other catalysts had charge values lower than that of the Pd catalyst. Therefore, the BiPd and PdBi catalysts will have a higher EAS compared to the other catalysts; the presence of Bi improved the exposed surface area of the Pd catalysts.

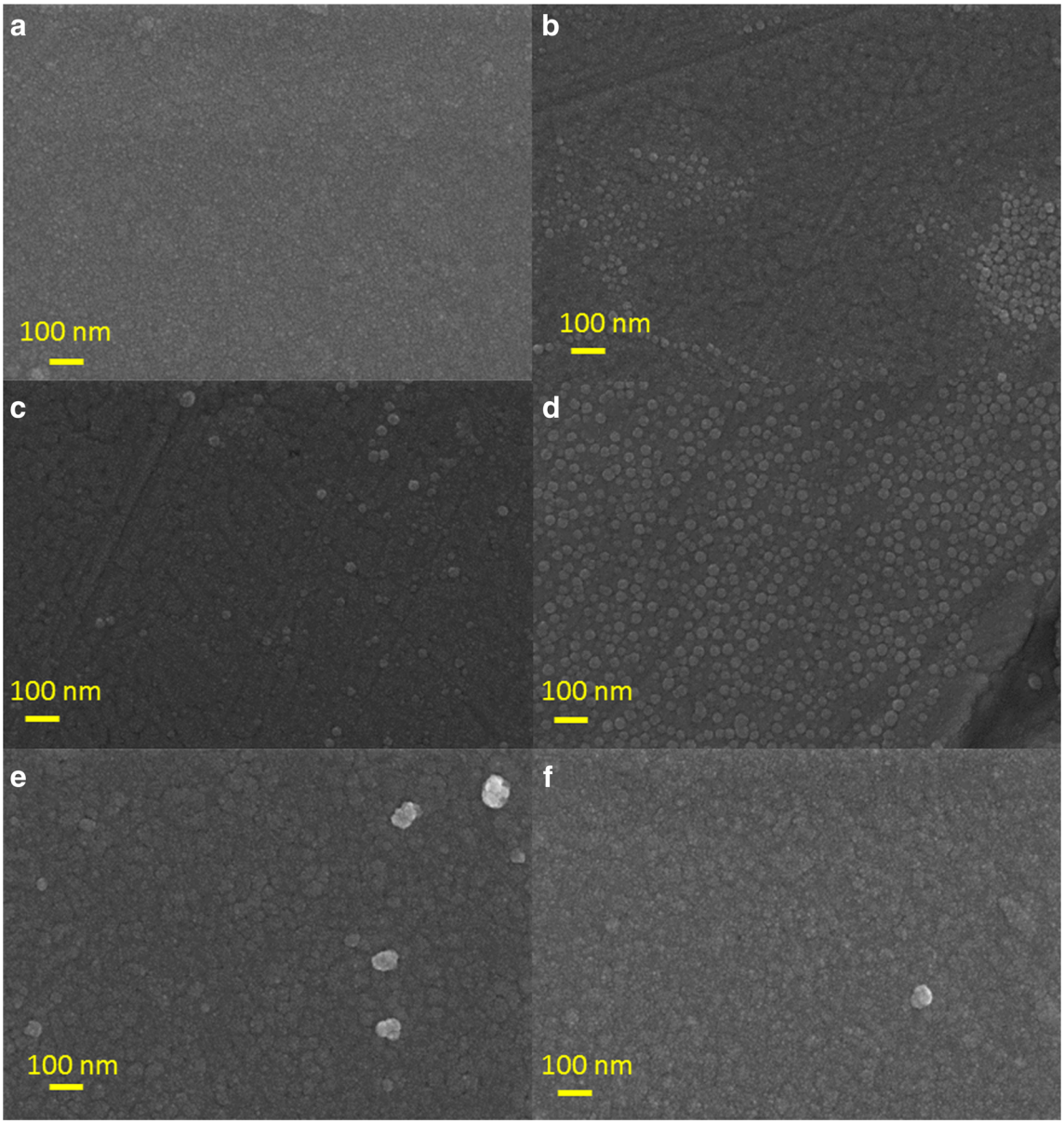

Fig. 3 SEM images of **a** Pd 25, **b** Pd 50, **c** PdSn, **d** SnPd, **e** PdBi and **f** PdBiSn 25

$$\mathrm{EAS}\left(\mathrm{m}^2\mathrm{g}_{\mathrm{Pd}}^{-1}\right) = \frac{\mathrm{Q_r}}{(4.24\ \mathrm{cm}^{-2} \times \mathrm{W_{Pd}})\mathrm{Ag}(\mathrm{cm}^2)} \quad (1)$$

Q_R Reduction charge
W_{Pd} Pd loading mass in grams
A_g Geometry of the surface area

Ethanol Electro-Oxidation

The activity of the prepared catalysts towards ethanol electro-oxidation reaction (EOR) was investigated using cyclic voltammetry in 0.1 M KOH solution and 0.1 M EtOH and is shown in Fig. 6 and the summary of the results shown in Table 2. The forward scan of the CV curves for all the catalysts had lower peak current than the reverse scans except for the PdBi catalysts. The BiPd catalysts showed no activity towards ethanol oxidation and therefore excluded for further studies due to Bi removal on the surface during Pd deposition. Pd catalyst exhibited the lowest peak current and broader peaks compared to all the other catalysts for the forward reaction, indicating a slow consumption of EtOH on the catalyst [11, 33]. The highest peak currents were observed from the SnPd and SnBiPd 25 catalysts for the reverse CV scan, these two materials showed the same activity for EOR, and also had the same interaction with KOH. The sharpness and rapid increase in peak currents is due to the fast removal of the adsorbed acetate intermediate species that were partially oxidised

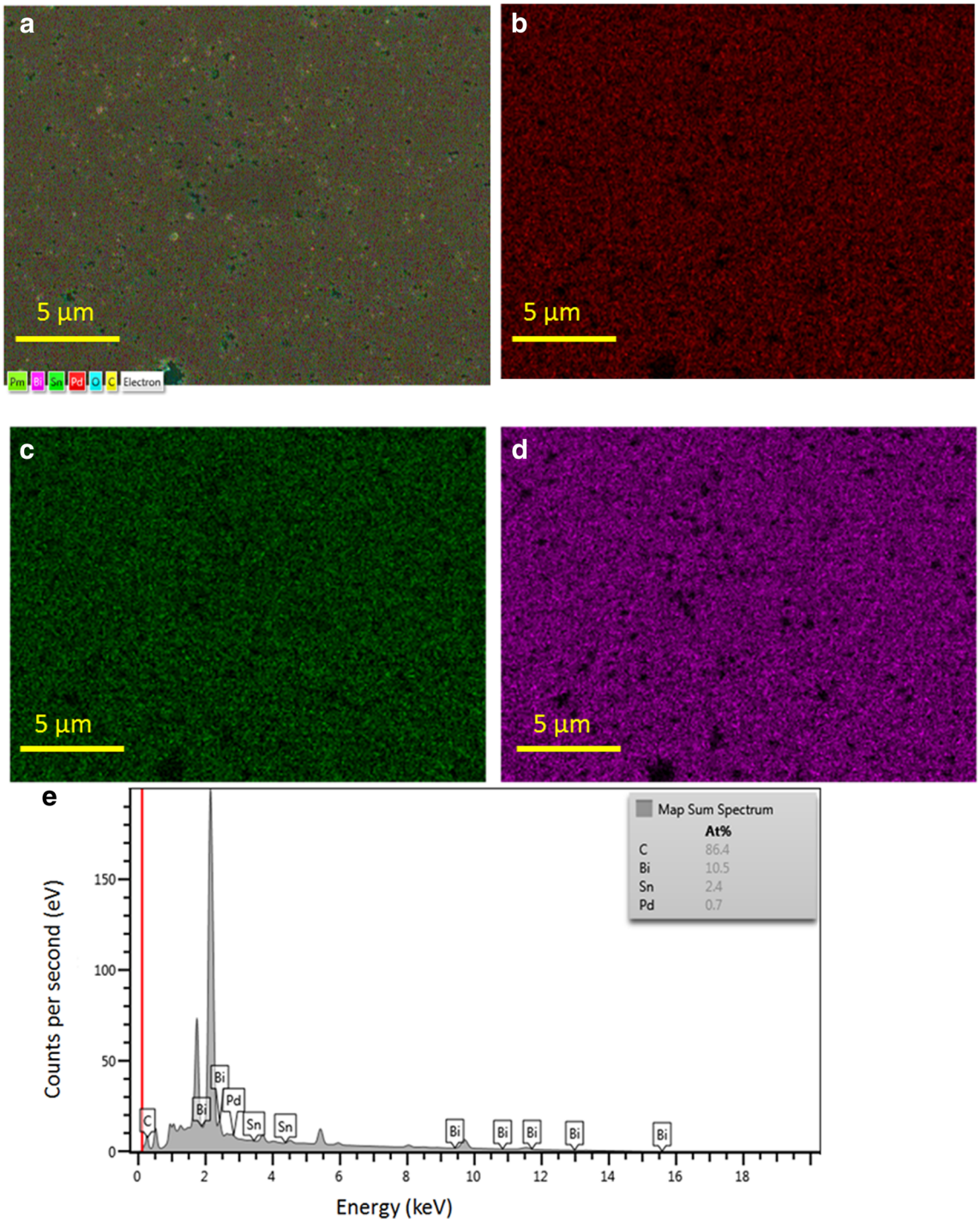

Fig. 4 Elemental map and EDS spectra of PdBiSn 25 catalyst showing: **a** Overlaid image; **b** Pd; **c** Sn; **d** Bi

during the forward reaction. This is the rate-limiting step for EOR as shown in Eqs. 2–5 where Eq. 5 shows the rate-limiting step [8, 11].

$$Pd + OH^- \rightarrow Pd{-}OH_{ads} + e^- \quad (2)$$

$$Pd + CH_3CH_2OH \rightarrow Pd{-}(CH_3CH_2OH)_{ads} \quad (3)$$

$$Pd{-}(CH_3CH_2OH)_{ads} + 3OH^- \rightarrow Pd{-}(CH_3CO)_{ads} + 3H_2O + 3e^- \quad (4)$$

$$Pd{-}(CH_3CO)_{ads} + Pd{-}OH_{ads} + OH^- \rightarrow CH_3COO^- + 2Pd + H_2O \quad (5)$$

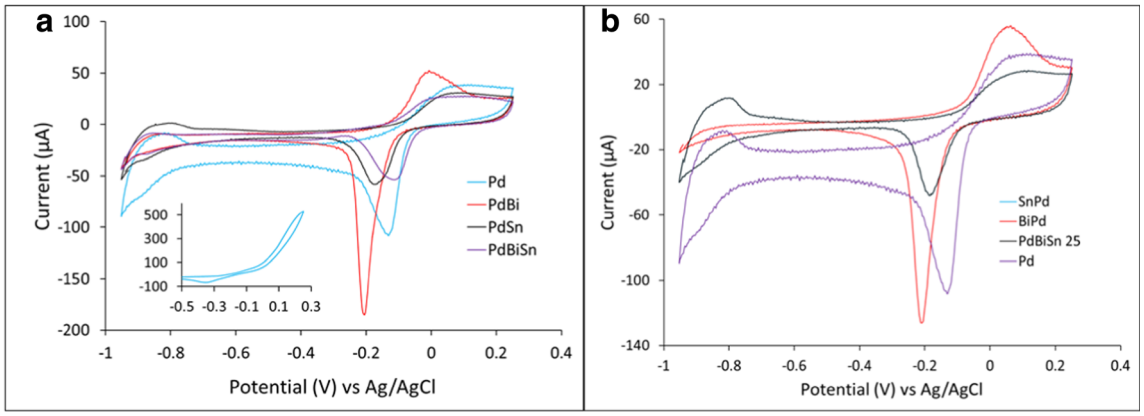

Fig.5 **a** Cyclic voltammogram of Pd, PdBi, PdSn and PdBiSn catalysts, **b** cyclic voltammogram of Pd, BiPd, SnPd and PdBiSn 25 catalysts in 0.1 M KOH at a scan rate of 10 mV/s

The CVs in Fig. 6a, b show the onset potential for the EOR reaction for the different catalysts. The onset potential for Pd, PdBi, PdSn, SnPd, PdBiSn 25 and PdBiSn 30 catalysts is − 0.37 V, − 0.46 V, − 0.46 V, − 0.50 V, − 0.50 V and − 0.53 V respectively. These results show that modifying Pd with either Sn or Bi improved catalytic activity due to the more negative onset of EOR on the binary and ternary catalysts compared to Pd catalyst; this is in agreement with literature [34, 35]. The similarities between PdBi and PdSn activities could be due to the similar chemical properties of Sn and Bi. While the PdBiSn 25 catalyst showed higher activity due to the presence of both Sn and Bi. The earliest onset potential was found on PbBiSn 30 material as expected because this material contains more Pd (30× deposition cycles) than the others (25× deposition cycles).

The PdSn and SnPd catalysts in Fig. 6c showed that SnPd catalysts had the highest $I_{forward}$ and $I_{reverse}$ compared to PdSn, as well as the sharper $I_{reverse}$ peak, indicating that it removes the adsorbed carbonate species much faster than PdSn does as discussed in literature [36]. PdBiSn 30 catalyst had a slower

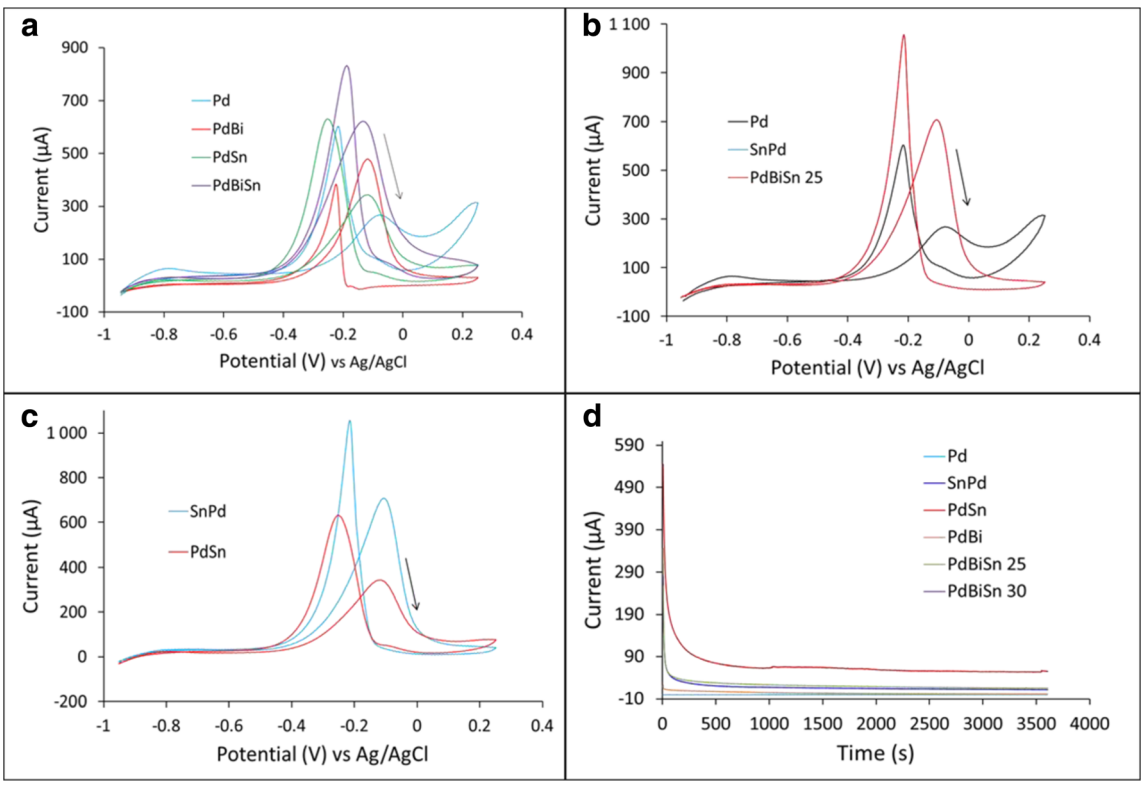

Fig.6 **a** Cyclic voltammogram of Pd, PdBi, PdSn and PdBiSn catalysts; **b** cyclic voltammogram of Pd, SnPd and PdBiSn 25 catalysts; **c** cyclic voltammograms for the ethanol comparison of PdSn and SnPd catalysts; **d** chronoamperometric curves at − 0.2 V of ethanol electrooxidation in 0.1 M KOH + 0.1 M EtOH. (Scan rate of 10 mV/s was used)

Table 2 Summary of ethanol electro-oxidation parameters for the different catalysts

Catalyst	Ethanol onset potential (V)	Ethanol ($I_{forward}/I_{reverse}$)
Pd	− 0.37	0.44
PdSn	− 0.46	0.55
PdBi	− 0.46	1.25
PdBiSn 30	− 0.53	0.74
SnPd	− 0.50	0.67
PdBiSn 25	− 0.50	0.67

ethanol oxidation due to broader peak for forward scan. The rapid drop of current observed for PdBiSn 25 indicates a faster EOR, accompanied by a sharp increase for the reverse scan indicating faster by product removal. The ratio of the reverse current and forward current ($I_{forward}/I_{reverse}$) is shown in Table 2,with the highest obtained from PdBi catalyst compared to all the other catalysts, and this was the better catalyst because it was able to achieve good activity and the least susceptible to poisoning. The highest value of 1.25 was obtained for PdBi catalyst followed by PdBiSn 30 with 0.74.

Chronoamperometry scans illustrating the stability of the catalysts in ethanol at − 0.2 V is shown in Fig. 6d. The initial high current decreased rapidly within the first 60 s, followed by a gradual decrease over time as the catalysts get poisoned. The highest current was obtained for PdBiSn 30 catalyst over 60 min. The order of the catalysts stability based on current was found to be PdBiSn 30>PdSn>PdBiSn 25>SnPd>PdBi>Pd. Pd catalyst was found to be the most susceptible towards poisoning, and the addition of both Sn and Bi improved the stability of the catalyst, which supports the bifunctional mechanism stated in literature [36, 37].

Conclusion

Pd-based binary and ternary catalysts were prepared using underpotential deposition method and tested for the electro-oxidation of ethanol in alkaline electrolyte. Sn and Bi were used as second or/and third metal to form binary and ternary Pd-based catalysts. Pd catalysts were deposited using Cu SLRR method while Sn and Bi were directly deposited at UPD. These materials were found to exhibit similar morphology with the exception of PdBi material. The addition of Sn and Bi to Pd was found to improve activity of the catalysts for ethanol oxidation, and also makes these catalysts least susceptible to poisoning. The addition of both Sn and Bi improved the catalysts stability in ethanol electro-oxidation. This work demonstrated that the addition of Sn and Bi on Pd catalyst can effectively lower the cost of fuel cell catalysts without compromising catalyst performance.

Acknowledgements National Centre for Nano-Structured Materials of the CSIR is acknowledged for the acquisition of SEM/EDS and FIB-SEM images.

Funding Information This work was funded by the US Air Force Office of Scientific Research (AFOSR) under Dr. Ali Sayir Program grant number FA9550-16-1-0060 and the CSIR-UWC cooperation fund.

References

1. E. Antolini, E. Gonzalez, Alkaline direct alcohol fuel cells. J. Power Sources **195**(11), 3431–3450 (2010)
2. M. Cifrain, K. Kordesch, Handbook of fuel cells, (2003)
3. N. Markovic, H. Gasteiger, P.N. Ross, Kinetics of oxygen reduction on Pt(hkl) electrodes: implications for the crystallite size effect with supported Pt electrocatalysts. J. Electrochem. Soc. **144**(5), 1591–1597 (1997)
4. B. Blizanac, P. Ross, N. Markovic, Oxygen electroreduction on Ag(111): the pH effect. Electrochim. Acta **52**(6), 2264–2271 (2007)
5. M. Kamarudin, S.K. Kamarudin, M. Masdar, W.R.W. Daud, Review: direct ethanol fuel cells. Int. J. Hydrog. Energy **38**(22), 9438–9453 (2013)
6. J. Friedl, U. Stimming, Model catalyst studies on hydrogen and ethanol oxidation for fuel cells. Electrochim. Acta **101**, 41–58 (2013)
7. B. Braunchweig, D. Hibbitts, M. Neurock, A. Wieckowski, Electrocatalysis: a direct alcohol fuel cell and surface science perspective. Catal. Today **202**, 197–209 (2013)
8. L. Zhang, Q. Chang, H. Chen, M. Shao, Recent advances in palladium-based electrocatalysts for fuel cell reactions and hydrogen evolution reaction. Nano Energy **29**, 198–219 (2016)
9. A. Zalineeva, A. Serov, M. Padilla, U. Martinez, K. Artyushkova, S. Baranton, C. Coutanceau, P.B. Atanassov, Self-supported pdxbi catalysts for the electrooxidation of glycerol in alkaline media. J. Am. Chem. Soc. **136**(10), 3937–3945 (2014)
10. Q. Yi, H. Chu, Q. Chen, Z. Yang, X. Liu, High performance Pd, PdNi, PdSn and PdSnNi nanocatalysts supported on carbon nanotubes for electrooxidation of C2C4 alcohols. Electroanalysis **27**, 388–397 (2015)
11. Y.-Y. Feng, Z.-H. Liu, Y. Xu, P. Wang, W.-H. Wang, D.-S. Kong, Highly active PdAu alloy catalysts for ethanol electro-oxidation. J. Power Sources **232**, 99–105 (2013)
12. R.M. Modibedi, E.K. Louw, K.I. Ozoemena, M.K. Mathe, The electrochemical atomic layer deposition of Pt and Pd nanoparticles on Ni foam for the electro-oxidation of alcohols. ECS Trans. **50**(21), 9–18 (2013)
13. R.M. Modibedi, T. Masombuka, M.K. Mathe, Carbon supported Pd–Sn and Pd–Ru–Sn nanocatalysts for ethanol electro-oxidation in alkaline medium. Int. J. Hydrog. Energy **36**(8), 4664–4672 (2011)
14. J. Cai, Y. Huang, Y. Guo, Bi-modified Pd/C catalyst via irreversible adsorption and its catalytic activity for ethanol oxidation in alkaline medium. Electrochim. Acta **99**, 22–29 (2013)
15. A. Dutta, S.S. Mahapatra, J. Datta, High performance PtPdAu nano-catalyst for ethanol oxidation in alkaline media for fuel cell applications. Int. J. Hydrog. Energy **36**(22), 14898–14906 (2011)
16. A. Dutta, A. Mondal, P. Broekmann, J. Datta, Optimal level of Au nanoparticles on Pd nanostructures providing remarkable electrocatalysis in direct ethanol fuel cell. J. Power Sources **361**, 276–284 (2017)

17. B.W. Gregory, D.W. Suggs, J.L. Stickney, Conditions for the deposition of CdTe by electrochemical atomic layer epitaxy. J. Electrochem. Soc. **138**(5), 1279–1284 (1991)
18. R. Hoyer, L. Kibler, D. Kolb, The initial stages of palladium deposition onto Pt(1 1 1). Electrochim. Acta **49**(1), 63–72 (2003)
19. L. Kibler, A. El-Aziz, D. Kolb, J. Mol, Electrochemical behaviour of pseudomorphic overlayers: Pd on Au(1 1 1). Catal. A: Chem. **199**(1–2), 57–63 (2003)
20. L. Kibler, M. Kleinert, D. Kolb, Initial stages of Pd deposition on Au(hkl). Surf. Sci. **461**(1–3), 155–167 (2000)
21. J. Tang, M. Petri, L. Kibler, D. Kolb, Pd deposition onto Au(111) electrodes from sulphuric acid solution. Electrochim. Acta **51**(1), 125–132 (2005)
22. A. El-Aziz, L. Kibler, Influence of steps on the electrochemical oxidation of CO adlayers on Pd(111) and on Pd films electrodeposited onto Au(111). J. Electroanal. Chem. **534**(2), 107–114 (2002)
23. L. Kibler, M. Kleinert, R. Randler, D. Kolb, Initial stages of Pd deposition on Au(hkl) Part I: Pd on Au(111). Surf. Sci. **443**(1–2), 19–30 (1999)
24. G. Hoogers, *Fuel Cell Technology Handbook* (CRC press, 2002)
25. M. Carmo, G. Doubek, R.C. Sekol, M. Linardi, A.D. Taylor, Development and electrochemical studies of membrane electrode assemblies for polymer electrolyte alkaline fuel cells using FAA membrane and ionomer. J. Power Sources **230**, 169–175 (2013)
26. T.S. Mkwizu, M.K. Mathe, I. Cukrowski, Electrodeposition of multilayered bimetallic nanoclusters of ruthenium and platinum via surface-limited redox−replacement reactions for electrocatalytic applications. Languir **26**(1), 570–580 (2010)
27. L.B. Sheridan, J. Czerwiniski, N. Jayaraju, D.K. Gebregziabiher, J.L. Stickney, D.B. Robinson, M.P. Soriaga, Electrochemical Atomic layer deposition (E-ALD) of palladium nanofilms by surface limited redox replacement (SLRR), with EDTA complexation. Electrocatalysis **3**(2), 96–107 (2012)
28. L.B. Sheridan, D.K. Gebregziabiher, J.L. Stickney, D.B. Robinson, Formation of palladium nanofilms using electrochemical atomic layer deposition (E-ALD) with chloride complexation. Langmuir **29**(5), 1592–1600 (2013)
29. J.M. Czerniawski, J.L. Stickney, Electrodeposition of In2Se3 using potential pulse atomic layer deposition. J. Phys. Chem. C **120**(29), 16162–16167 (2016)
30. J. Aldana-Gonzalez, J. Olvera-Garcia, M.M. De Oca, M. Romero-Romo, M. Ramirez-Silva, M. Palomar-Pardave, Electrochemical quantification of the electro-active surface area of Au nanoparticles supported onto an ITO electrode by means of Cu upd. Electrochem. Commun. **56**, 70–74 (2015)
31. Y. Chen, L. Wang, A. Pradel, A. Merlen, M. Ribes, M.-C. Record, Underpotential deposition of selenium and antimony on gold. J. Solid State Electrochem. **19**(8), 2399–2411 (2015)
32. R.A. Hameed, Facile preparation of Pd-metal oxide/C electrocatalysts and their application in the electrocatalytic oxidation of ethanol. Appl. Surf. Sci. **411**, 91–104 (2017)
33. B. Pierozynski, T. Mikolajczyk, M. Turemko, On the temperature performance of ethanol oxidation reaction at palladium-activated nickel foam. Electrocatalysis **6**(2), 173–178 (2015)
34. Y.-Y. Feng, Z.-H. Liu, W.-Q. Kong, Q.-Y. Yin, L.-X. Du, Promotion of palladium catalysis by silver for ethanol electro-oxidation in alkaline electrolyte. Int. J. Hydrog. Energy **39**(6), 2497–2504 (2014)
35. Y. Zhang, Q. Yi, Z. Deng, X. Zhou, H. Nie, Excellent electroactivity of ternary Pd–Ag–Sn nanocatalysts for ethanol oxidation. Catal. Lett. **148**(4), 1190–1201 (2018)
36. L. Karuppasamy, S. Anandan, C.-Y. Chen, J.J. Wu, Sonochemical synthesis of PdAg/RGO nanocomposite as an efficient electrocatalyst for both ethanol oxidation and oxygen reduction reaction with high CO tolerance. Electrocatalysis **8**(5), 430–441 (2017)
37. R.M. Modibedi, K.I. Ozoemena, M.K. Mathe, *Electrocatalysis*, (Springer, 2013), pp. 129–156